Research Square

Preprints are preliminary reports that have not undergone peer review.
They should not be considered conclusive, used to inform clinical practice,
or referenced by the media as validated information.

Influence of β-Sitosterol Incorporation on the Physicochemical Properties, Drug Release, and Stability of Doxorubicin-Loaded Liposomes

Bhavinkumar Sureshchandra Dave
Parul University
Rajesh Dodiya
rajesh.dodiya24770@paruluniversity.ac.in

Parul University
Avik Parekh
The Charutar Vidya Mandal (CVM) University

Research Article

Keywords: Doxorubicin, β-sitosterol, lysophosphatidylcholine, bilayer stability, sustained drug release

Posted Date: November 26th, 2026

DOI: https://doi.org/10.21203/rs.3.rs-11499813/v1

License: This work is licensed under a Creative Commons Attribution 4.0 International License.
Read Full License

Additional Declarations: No competing interests reported.

Influence of β-Sitosterol Incorporation on the Physicochemical Properties, Drug Release, and Stability of Doxorubicin-Loaded Liposomes

Author Names

Bhavinkumar Sureshchandra Dave[a], Rajesh Dodiya[a,*], Avik Parekh[b]

Institutional Affiliations

[a] Faculty of Pharmacy, Parul University, P.O. Limda, Ta. Waghodia – 391760, Dist. Vadodara, Gujarat, India
[b]Department of Biotechnology, Institute of Science & Technology for Advanced Studies & Research (ISTAR), The Charutar Vidya Mandal (CVM) University, Vallabh Vidyanagar – 388120, Gujarat, India

Corresponding Author Information

Dr. Rajesh Dodiya

- **Affiliation:** Faculty of Pharmacy, Parul University, P.O. Limda, Ta. Waghodia – 391760, Dist. Vadodara, Gujarat, India
- **E-mail:** rajesh.dodiya24770@paruluniversity.ac.in

Author ORCID iDs

- Bhavinkumar Sureshchandra Dave: [ORCID ID: 0009-0006-9808-9745]
- Rajesh Dodiya: [ORCID ID: 0000-0002-0533-2210]
- Avik Parekh: [ORCID ID: 0009-0001-8683-0798]

ABSTRACT

• **Purpose:** Encapsulating doxorubicin within lipid nanocarriers drastically mitigates its dose-limiting cardiotoxicity; however, conventional cholesterol matrices frequently suffer from shelf-life leakage and rapid membrane hydrolytic degradation. This investigation sought to optimize the structural stability of the bilayer by substituting traditional cholesterol with the plant-derived sterol, β-sitosterol. The primary goal was to enhance long-term membrane integrity, suppress the generation of lipid impurities, and secure a highly controlled transmembrane diffusion rate without compromising the protective benefits of liposomal encapsulation.

• **Methods:** Vesicles were fabricated using an ethanol injection approach. Dynamic light scattering and asymmetric flow field-flow fractionation (AF4) were deployed orthogonally to evaluate hydrodynamic profiles and physical uniformity. Microstructural contours were verified using cryogenic transmission electron microscopy (cryo-TEM). Phospholipid breakdown was quantified by monitoring lysophosphatidylcholine (Lyso-PC) accumulation over a six-month storage window at 25°C. In vitro transport mechanics, human plasma compatibility, and antiproliferative potencies against human breast adenocarcinoma cells (MCF-7) were thoroughly characterized via dissolution assays, serum retention models, MTT viability tracks, and scratch-migration wounds.

• **Results:** The engineered β-sitosterol framework yielded a highly uniform vesicle cohort (99 ± 6 nm) with an exceptional active drug entrapment yield of 97.90%. Calorimetric thermograms linked the phytosterol integration with enhanced molecular packing and a distinct phase behavior change (Δ H = 479.0 kJ/mol). Crucially, the formulation effectively blocked hydrolytic cleavage pathways, limiting Lyso-PC mass accumulation to a minimal 2.81% after 180 days. While maintaining structural robustness in human plasma, the optimized vehicle generated a steady, diffusion-controlled release profile and lowered the half-maximal inhibitory threshold (IC_{50}) against MCF-7 lines to 1174 nM, markedly outperforming the commercial liposomal benchmark (2420 nM).

• **Conclusion:** These findings demonstrate that substituting cholesterol with β-sitosterol provides superior bilayer packing and drastically lowers lipid degradation parameters over prolonged storage. This sterol manipulation strategy offers a highly stable, structurally robust alternative matrix for optimizing the delivery and therapeutic performance of anthracycline nanomedicines.

Key words: Doxorubicin; β-sitosterol; lysophosphatidylcholine; bilayer stability; sustained drug release.

1.0 INTRODUCTION

Doxorubicin remains an indispensable cornerstone within clinical oncology regimes, demonstrating broad-spectrum efficacy against leukemia, breast adenocarcinomas, and diverse solid malignancies [1]. Unfortunately, the therapeutic utility of this potent anthracycline antibiotic is severely bottlenecked by its narrow therapeutic index and catastrophic, dose-dependent side effects most notably irreversible cardiomyopathy [1] [2]. Furthermore, its rapid systemic clearance and non-specific tissue distribution frequently compromise therapeutic outcomes while intensifying off-target systemic toxicities.

To shield healthy tissues from toxic concentrations while optimizing therapeutic delivery, liposomal nanocarriers have emerged as highly successful intervention platforms[2]. Encapsulating anthracyclines within self-assembled lipid vesicles radically alters their pharmacokinetic trajectories and prolongs vascular circulation lifetimes. This structural shielding facilitates preferential accumulation within malignant tumors via the compromised vasculatures of target tissues a phenomenon widely recognized as the enhanced permeability and retention (EPR) effect.

While first-generation pegylated doxorubicin liposomes have achieved widespread clinical success, substantial engineering challenges persist regarding their physical and chemical stability profiles [2] [3]. The clinical and commercial viability of these nanomedicines is frequently compromised by premature drug leakage during long-term storage and the chemical degradation of the underlying lipid matrix. Phosphatidylcholine the primary building block of hydrogenated soy phosphatidylcholine (HSPC) is highly susceptible to spontaneous chemical hydrolysis. This degradation pathway yields lysophosphatidylcholine (Lyso-PC) impurities, which rapidly destabilize the vesicle architecture, fluidize the tightly packed membrane boundaries, and trigger uncontrolled payload dumping before the drug reaches its intended target site.

Traditionally, cholesterol is incorporated into liposomal bilayers to act as a mechanical buffer, regulating interfacial fluidity, reducing permeability, and reinforcing membrane rigidity[4]. Nevertheless, contemporary lipid engineering suggests that alternative sterol frameworks can introduce distinct structural advantages. The plant-derived phytosterol β-sitosterol shares close structural homology with cholesterol but possesses an extended ethyl chain modification on its hydrophobic tail. Recent biophysical investigations indicate that this extended side-chain architecture allows β-sitosterol to interdigitate uniquely within phospholipid matrices, promoting tighter molecular packing densities and dampening membrane fluctuations more effectively than animal cholesterol[4] [5]. Consequently, substituting cholesterol with β-sitosterol offers a promising strategy to enhance lipid bilayer ordering and suppress the hydrolytic water penetration that drives Lyso-PC impurity formation.

The physical parameters and structural homogeneity of these vesicles are also heavily dictated by the underlying engineering methodology. Among conventional production techniques, the ethanol injection method offers a highly reproducible, single-step, and scalable approach to generate small, monodisperse lipid nanocarriers without relying on harsh mechanical stresses [6]. However, fine-tuning the particle dimensions and managing molecular packing within the resulting thin films requires a precise, harmonious balance between the process settings and the specific lipid-to-sterol blending ratios.

To address these current challenges, this investigation systematically explores the architectural benefits of substituting cholesterol with β-sitosterol in doxorubicin-loaded liposomes fabricated via ethanol injection. Rather than targeting a divergence in cardiotoxicity mitigation—which remains a fundamental benefit of the liposomal carrier itself—this work focuses on resolving membrane integrity flaws and lipid stability challenges.
The engineered nanocarriers were comprehensively evaluated using dynamic light scattering (DLS), cryogenic transmission electron microscopy (cryo-TEM), and high-resolution asymmetric flow field-flow fractionation (AF4) under non-destructive laminar flow fields. Additionally, we tracked the long-term chemical resilience of the membranes by monitoring Lyso-PC accumulation over a six-month stability challenge. Finally, the real-world utility of the optimized carrier was validated through *in vitro* transport kinetics, human plasma retention

profiles, and dose-dependent antiproliferative and anti-migratory evaluations using MCF-7 human breast cancer models.

2.0 MATERIALS AND METHODS

2.1 Chemicals, Reagents, and Biological Materials

Doxorubicin, sucrose, cholesterol, and 3-(4,5-dimethylthiazol-2-yl)-2,5-diphenyltetrazolium bromide (MTT) were supplied by Sigma-Aldrich (St. Louis, MO, USA). Lipoid GmbH (Ludwigshafen, Germany) provided the lipids, which consisted of lysophosphatidylcholine (Lyso-PC), methoxy-poly(ethylene glycol)–distearoyl phosphatidylethanolamine (mPEG-DSPE), and hydrogenated soy phosphatidylcholine (HSPC). Hi-Media Laboratories (Mumbai, India) was the source for β-sitosterol (BS). Merck (Darmstadt, Germany) supplied the organic solvents (chloroform, methanol, and acetonitrile), whereas dibasic potassium phosphate was purchased from Merck.

Unless stated otherwise, remaining reagents and chemicals were analytical grade or better, sourced commercially.

The National Centre for Cell Science (Pune, India) provided the human breast cancer cell line MCF-7. Cell maintenance was conducted at 37 °C in a humidified 5% CO_2 environment using high-glucose DMEM. This media was supplemented with 12% fetal bovine serum alongside 1% penicillin-streptomycin containing 100 U/mL of each antibiotic.

2.2 Preparation Methodology for Lipid Nanocarriers

Encapsulation of doxorubicin HCl (DOX) inside the lipid vesicles was achieved via an ethanol injection approach[6] . First, we precisely weighed the lipophilic ingredients specifically cholesterol, β-sitosterol, mPEG-DSPE, and HSPC to match the specific molar proportions detailed in Table 1. This lipid blend was dissolved in ethanol inside a glass vessel under constant agitation, keeping the system at a stable temperature of 65 °C. In a separate container, an aqueous phase consisting of an ammonium sulfate solution was prepared. We then slowly introduced the ethanolic lipid phase into the ammonium sulfate solution while maintaining continuous stirring, allowing the resulting mixture to agitate for an additional 30 minutes at 65 °C. To control the dimensions of the vesicles, the liposomal fluid was forced through polycarbonate membrane filters until an average vesicle size between 80 and 100 nm was reached[7]. Dynamic light scattering measurements tracked the size profile after successive passes to confirm when the target distribution was successfully established.

To establish the active loading environment, the raw liposomal suspension underwent dialysis against a 10% sucrose matrix, purging unencapsulated ammonium sulfate from the continuous phase. We verified the complete elimination of external sulfate ions by reacting an aliquot of the dialysate with a barium chloride solution; the absence of a white barium sulfate precipitate confirmed successful purification. Separately, doxorubicin hydrochloride was brought to 60 °C after dissolution in a 10% sucrose medium. Following the addition of an adequate quantity of histidine buffer, this heated drug solution was combined with the dialyzed vesicle suspension. This combined system was incubated at 60 °C for 1 hour, driving DOX migration into the core via the pre-established transmembrane ammonium sulfate gradient[7] [8] . Following active loading, the formulation was chilled to a temperature range of 2–8 °C for 1 hour. We then adjusted the batch to its final target volume using the 10% sucrose solution, brought the final

pH to 6.65 using a dilute sodium hydroxide solution, and passed the doxorubicin liposomes through a 0.2 μm membrane filter for sterilization.

Table 1: Molar variations of cholesterol and β-sitosterol across five liposomal doxorubicin batches.

Formulation Code	Fixed Lipid Matrix (mg/mL)		Variable Sterol Phase mg/mL		Active Drug (mg/mL)
	MPEG-DSPE	HSPC	Cholesterol	B-sitosterol	Doxorubicin HCl
L-DOX A	3.19	9.58	3.19	0.00	2.00
L-DOX B	3.19	9.58	2.39	0.80	2.00
L-DOX C	3.19	9.58	1.60	1.60	2.00
L-DOX D	3.19	9.58	0.80	2.39	2.00
L-DOX E	3.19	9.58	0.00	3.19	2.00

2.3 Analytical Profiling of the Formulated Nanocarriers

2.3.1 DLS-Based Assessment of Hydrodynamic Size and Surface Charge

An evaluation of the particle size and polydispersity index (PDI) of the liposomal formulations was conducted using dynamic light scattering (DLS)[9] . To assess the colloidal stability of the engineered vesicles, we quantified their surface zeta potential[10] . Prior to loading into the instrument, each sample underwent appropriate dilution using double-distilled water. All data collection was carried out on a Zetasizer Nano ZS system (Malvern Instruments, UK) operating with a 633-nm laser source. To guarantee statistical reliability, measurements for each unique formulation batch were recorded in triplicate (n = 3). Elevated absolute values for zeta potential reflect robust electrostatic repulsion across the particulate boundaries, which fundamentally serves to inhibit vesicle aggregation[10] .

2.3.2 Hydrodynamic Separation and Characterization via AF4

To isolate and evaluate the liposomal structures according to their respective molecular weights and sizes under noninvasive laminar flow environments, we utilized asymmetric flow field-flow fractionation (AF4)[11] [12] .Because this high-resolution methodology operates without a stationary phase, it offers a distinct processing advantage for polydisperse or structurally delicate matrices like lipid vesicles[11], [12] .Fractionation experiments were executed on AF2000 separation module (Postnova) configured with a short seperation channel, a 350 μm channel spacer, and a semipermeable membrane made of 30 kDa regenerated cellulose. To protect the structural stability of the particles, sample delivery was handled via an autosampler thermal-regulated at 4°C. Downstream monitoring of the eluted components was achieved using a Shimadzu photodiode array detector. Preparation involved diluting the vesicle sample with a 10% sucrose matrix to reach a target concentration of 1000 μg/mL, followed by gentle manual swirling to guarantee uniform dispersion. We then passed this diluted liquid through a 0.1 μm membrane filter to clear any extraneous particulate contaminants. From this purified preparation, a 5 μL aliquot was introduced into the AF4 infrastructure to initiate the fractionation run.

2.3.3 Visual Morphological Evaluation via Cryo-TEM

Cryogenic transmission electron microscopy (Cryo-TEM) was utilized to inspect the structural and morphological features of the prepared liposomal batches[13] . To achieve swift vitrification, a 3 µL sample volume (adjusted to 1000 µg/mL) was loaded onto a carbon-coated TEM grid, blotted to establish a thin layer, and immediately plunge-frozen into liquid ethane[13] . Throughout the handling process, liquid nitrogen cooling was applied to keep the vitrified grid at a steady temperature below −165 °C. Finally, a specialized cryo-transfer mechanism was used to safely shift the chilled grid into the transmission electron microscope chamber for subsequent imaging[13] .

2.3.4 Evaluation of Drug Content and Encapsulation Efficiency

To evaluate the total doxorubicin payload, a 0.2 mL volume of the liposomal formulation (containing 4000 µg/mL DOX) was mixed with 20 mL of methanol supplemented with 0.1% (v/v) glacial acetic acid. This mixture was subjected to sonication before being processed via high-performance liquid chromatography (HPLC)[14] [15] . For the estimation of unencapsulated (free) doxorubicin, a 1 mL aliquot of the vesicle formulation was diluted into 10 mL of phosphate-buffered saline (PBS, pH 7.4) and ultracentrifuged at 60,000 rpm for 60 min at a controlled temperature of 10 °C. The resulting supernatant, which held the non-entrapped drug fraction, was isolated, combined with 0.1% (v/v) formic acid in methanol, and sonicated. This free active fraction was then quantified through HPLC analysis[14], [15] .

Chromatographic investigations were carried out on a Waters Alliance HPLC configuration complete with a mobile phase degassing unit, a binary pumping module, an automatic sampler, and a Waters 2489 UV/Vis detector. Analyte separation took place on a Hypersil BDS C18 column (150 × 4.6 mm, 5 µm) regulated at a stationary temperature of 30 °C. The mobile phase system comprised an isocratic mixture of acetonitrile and 0.01 M o-phosphoric acid in a 40:60 (v/v) ratio, with the final fluid pH adjusted to 2.0. Elution was performed at a constant flow rate of 0.75 mL/min over a total runtime of 20 min, while the monitoring wavelength was fixed at 234 nm[2], [14] .

2.3.5 Quantitative Profiling of Lipid Membrane Constituents

High-performance liquid chromatography (HPLC) was employed to establish the exact concentrations of individual lipid constituents, including mPEG-DSPE (319 µg/mL), HSPC (958 µg/mL), cholesterol (160 µg/mL), and β-sitosterol (160 µg/mL)[16], [17] . Chromatographic resolved fractions were achieved over a Zorbax Eclipse XDB-C18 column (100 × 4.6 mm, 5 µm; Agilent Technologies, USA) regulated at a working temperature of 40 °C. For the mobile phase, a mixture of water, methanol, tetrahydrofuran, and trifluoroacetic acid was blended in a 120:800:80:1 (v/v/v/v) volume ratio and run at a fixed flow rate of 2 mL/min. Monitoring of the eluted lipid species was carried out via a refractive index detector (RID) configured with a baseline sensitivity (1024) and an internal cell temperature (40 °C).

2.3.6 Differential Scanning Calorimetry (DSC) Analysis

To evaluate the thermal behavior of the lipid bilayer matrix, calorimetric characterization of the prepared liposomal systems was conducted on a Nano DSC, TA Instruments [18] . Roughly 300 µl of DOX-loaded vesicle solution (2000 µg/mL) was introduced into the active sample cell, while a matching volume of pure buffer solution was transferred to parallel reference cell.

We recorded the thermal profiles across a temperature span from 20 °C to 90 °C, utilizing a uniform heating velocity of 1 °C/min under an internal system pressure of 3 atm. Following necessary baseline subtraction protocols from the collected thermograms, the main phase transition temperature (Tm) was identified[18] .

2.3.7 Chromatographic Quantification of Lysophosphatidylcholine (Lyso-PC) Content

We evaluated the doxorubicin liposome formulation for the presence of oxidative and hydrolytic phospholipid impurities using high-performance liquid chromatography (HPLC) coupled with a refractive index (RI) detector[19] [20] . To isolate and quantify the lysophosphatidylcholine (Lyso-PC) fraction, we used a Luna C18(2) analytical column (250 × 4.6 mm, 5 µm; Phenomenex, USA). The internal column environment was kept steady at a temperature of 40 °C. Chromatographic migration was driven by an isocratic mobile phase composed of 10 mM ammonium formate buffer, formic acid, methanol, and tetrahydrofuran combined in a strict 200:1:750:50 (v/v/v/v) volume ratio.

2.3.8 Evaluation of In Vitro Drug Release Kinetics

We evaluated the elution profile of liposomal doxorubicin across a specialized dialysis setup following standard methodology[21] [22] . For this assay, we transferred a 1 mL volume of the prepared vesicle suspension (equating to a doxorubicin concentration of 1000 µg/mL) into a Float-A-Lyzer dialysis tube engineered with a 300 kDa molecular weight cutoff. This tube assembly was submerged inside a temperature-regulated, jacketed flask containing 500 mL of phosphate-buffered saline (PBS, pH 7.4) that had been supplemented with 0.5% Tween 80. The dissolution environment was kept stable at 37 °C under continuous agitation at 60 rpm.

At scheduled sampling points, we harvested 1-mL aliquots from the bulk media to measure the liberated drug fractions. Quantifying these doxorubicin concentrations required a Waters Alliance HPLC setup configured with a degassing module, binary pumping system, automatic sampler, and a Waters 2489 UV/Vis detector. Analyte resolution took place over a Hypersil BDS C18 stationary column (150 × 4.6 mm, 5 µm) maintained at 30 °C. The mobile phase comprised an isocratic blend of acetonitrile and 0.01 M o-phosphoric acid (40:60, v/v; pH 2.0). Chromatographic runs were executed at a flow velocity of 0.75 mL/min across a 20-min window, tracking the target peak at an absorbance wavelength of 234 nm.

2.3.9 In Vitro Scratch Assay for Cell Migration Assessment

We performed a scratch assay to evaluate how the optimized liposomal formulation (L-DOX C) affects the migration kinetics of MCF-7 human breast cancer cells[23] [24] . Sub-confluent MCF-7 cultures were grown in Petri dishes and exposed for 24 hours to sub-lethal concentrations of L-DOX C (below its determined IC_{50}, while the parallel control group was treated with blank liposomes. Following this initial incubation, we washed the cells and introduced a uniform, linear scratch across the monolayer using a sterile micro pipette tip to establish a cell free boundary gap.

The cultures were then maintained in a low-serum environment consisting of DMEM supplemented with 0.5% fetal bovine serum (FBS) for an additional 24 hours. At the conclusion of this period, the cells underwent fixation with methanol and staining with 0.5% crystal violet solution. Photomicrographs of the denuded wound region were documented at 0 and 24 hours.

To quantify wound closure, we measured the gap width at 25 distinct points per sample grid, calculating the final migration percentage by comparing the boundaries across the 24-hour window.

2.3.10 In Vitro Cytotoxicity Evaluation via MTT Assay

We evaluated the in vitro cytotoxic profiles of the optimized liposomal formulation (L-DOX C) against the commercial liposomal doxorubicin control using an MTT colorimetric assay[25], [26] . For this purpose, MCF-7 breast cancer cells at passage number 24 were seeded inside a 96-well culture plate at an initial density of 1 X 10^4 cells per well and incubated to allow surface attachment. Following adherence, we exposed the cell populations to both formulations across a doxorubicin concentration gradient spanning from 100 to 10,000 nM.

After a 24-hour treatment window, each well received a 50 µL aliquot of the MTT reagent (1 mg/mL), and the plates were incubated for an additional 3 to 4 hours to promote intracellular formazan crystallization. We then introduced 100 µL of dimethyl sulfoxide (DMSO) to solubilize these dark formazan crystals. Optical density was recorded at a detection wavelength of 570 nm utilizing an Epoch multi-well microplate reader. Finally, we calculated the absolute percentage of cell viability by benchmarking the treated sample optical densities against the values obtained from the unexposed control wells.

2.3.11 In Vitro Stability and Drug Retention Profile in Human Plasma

To confirm how well the optimized liposomal formulation holds up under biological conditions, we monitored doxorubicin retention alongside changes in particle size in the presence of human plasma[27], [28], [29] . Commercially sourced human plasma was combined with the liposomal suspension at a 1:100 dilution ratio. This step yielded a final doxorubicin concentration of 1 µg/mL within a matrix containing 50% human plasma. We incubated these preparation tubes at 37 °C under constant mechanical shaking at 150 rpm for a total duration of 24 hours. Sampling aliquots were collected at specific, scheduled intervals (0, 2, 4, 6, 8, 12, and 24 hours).

To isolate and measure the unencapsulated doxorubicin within these plasma matrices, we passed the gathered samples through PD-10 desalting columns. This separation step isolated the free active drug from the liposome-bound fraction. Following isolation, both drug retention and encapsulation profiles were evaluated using the same HPLC-based techniques described for our entrapment efficiency experiments. For the particle size measurements, we ran a centrifugation step at 80,000 rpm for 60 minutes at a stable temperature of 10 °C. The resulting pellets were isolated, washed three times with a phosphate buffer solution (pH 7.4), and fully resuspended in a 300 mM sucrose solution prior to hydrodynamic size tracking.

3.0 EXPERIMENTAL RESULTS AND SCIENTIFIC DISCUSSION

3.1 Hydrodynamic Diameter, Homogeneity, and Surface Charge Dynamics

Based on our dynamic light scattering (DLS) investigations, all five doxorubicin-loaded liposomal formulations (L-DOX A through E) maintained highly uniform vesicle populations, evidenced by low polydispersity index (PDI) values spanning from 0.079 to 0.177[30] [31] . As detailed across Table 2 and Fig. 1, we observed a steady, progressive increase in the mean hydrodynamic diameter across the groups. Specifically, the diameter

expanded from 89 ± 6 nm for L-DOX A to 95 ± 5 nm for L-DOX B, 99 ± 6 nm for L-DOX C, 107 ± 8 nm for L-DOX D, and peaked at 111 ± 6 nm for L-DOX E(see Table 2, Fig. 1).. Furthermore, electrokinetic tracking revealed that every batch having a net negative surface charge ranging between −12.1 ± 4.66 mV and −16.5 ± 2.31 mV (see Table 2, Fig. 2).

These precise nanoscale dimensions and narrow distributions align closely with the structural targets optimized for efficient liposomal drug delivery vehicles[30] . Mechanistically, the uniform negative zeta potential profiles generate sufficient inter-particulate electrostatic repulsion to suppress aggregation over prolonged storage and systemic circulation. These combined physical traits confirm that our engineered nanocarriers successfully satisfy the standard size and homogeneity benchmarks required for stable, injectable formulations. We hypothesize that the incremental size increase observed with progressive β-sitosterol substitution stems from how individual sterol molecular architectures dictate lipid bilayer packing efficiencies. Because β-sitosterol possesses an extended ethyl side chain compared to cholesterol, it decreases the local packing density within the membrane, yielding slightly expanded vesicular volumes without undermining overall colloidal stability.

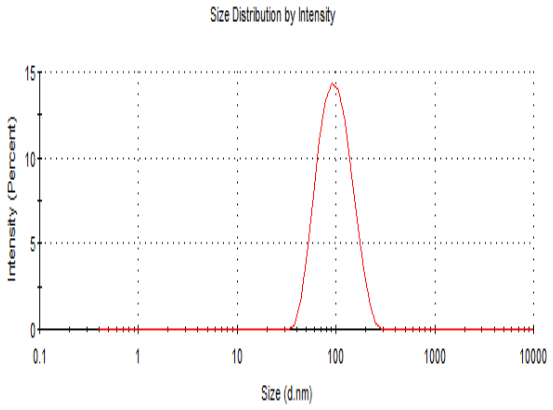

1(a)

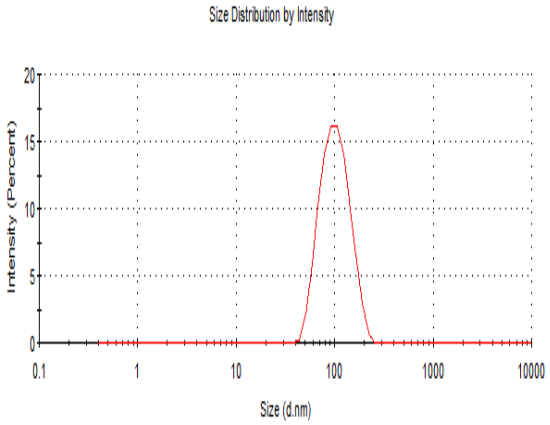

1(b)

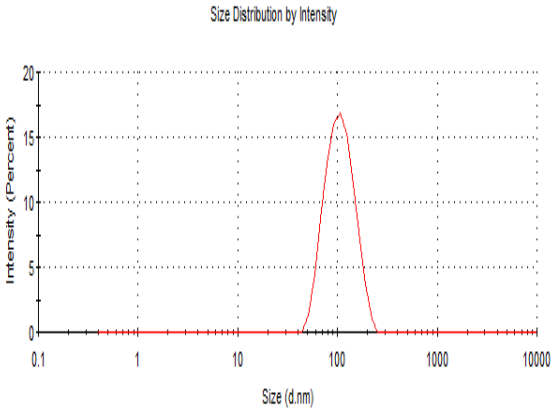

1(c)

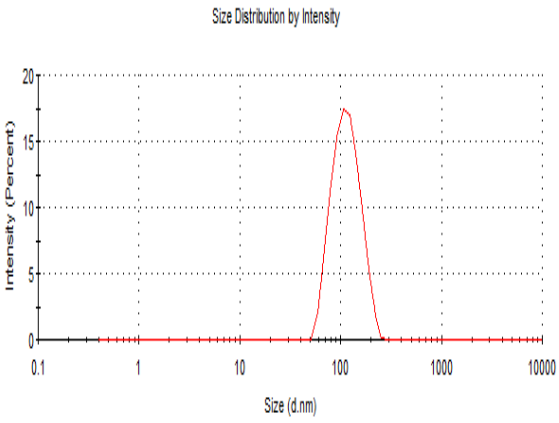

1(d)

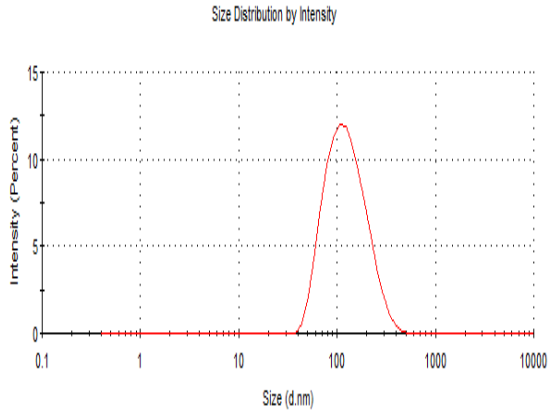

1(e)

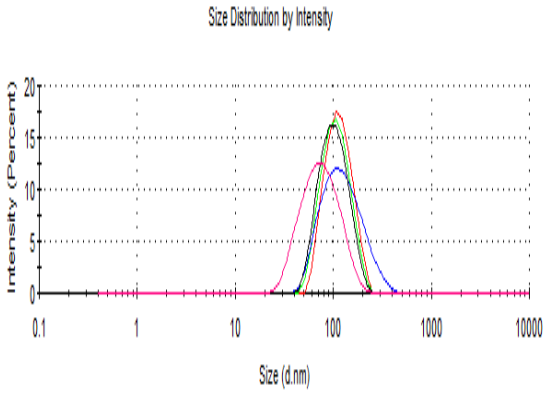

1(f)

Fig. 1: Size distribution graphs (a to e) L-DOX A to L-DOX E, and (f) Combined spectral overlay of the formulation variants.

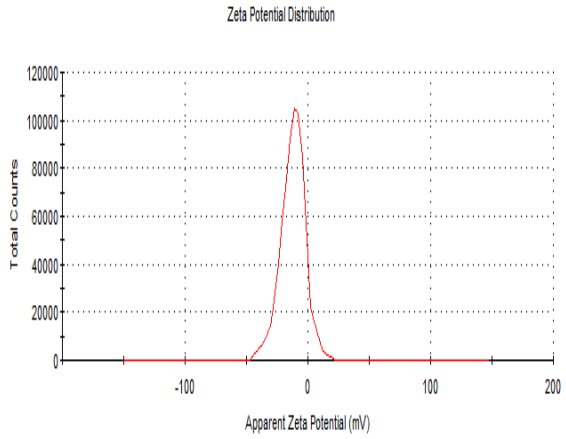

2(a)

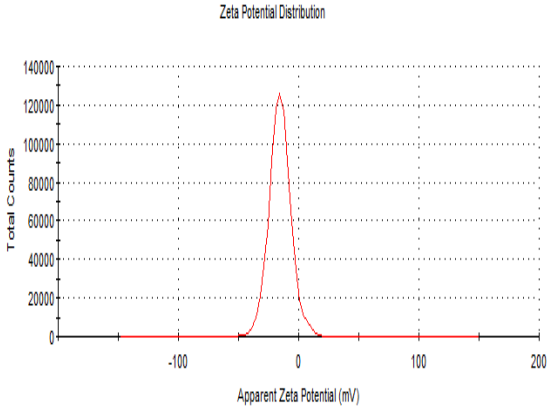

2(b)

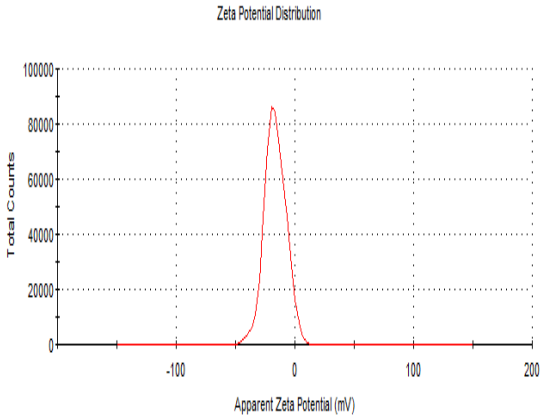

2(c)

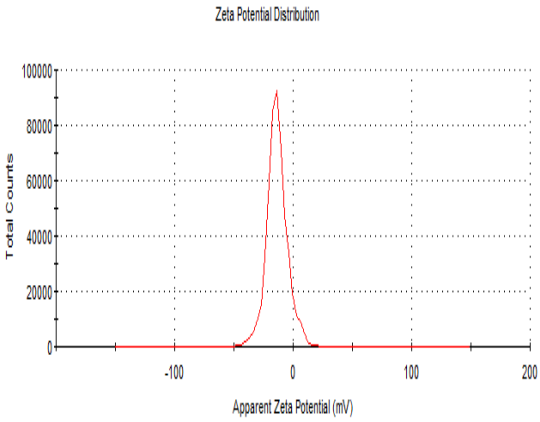

2(d)

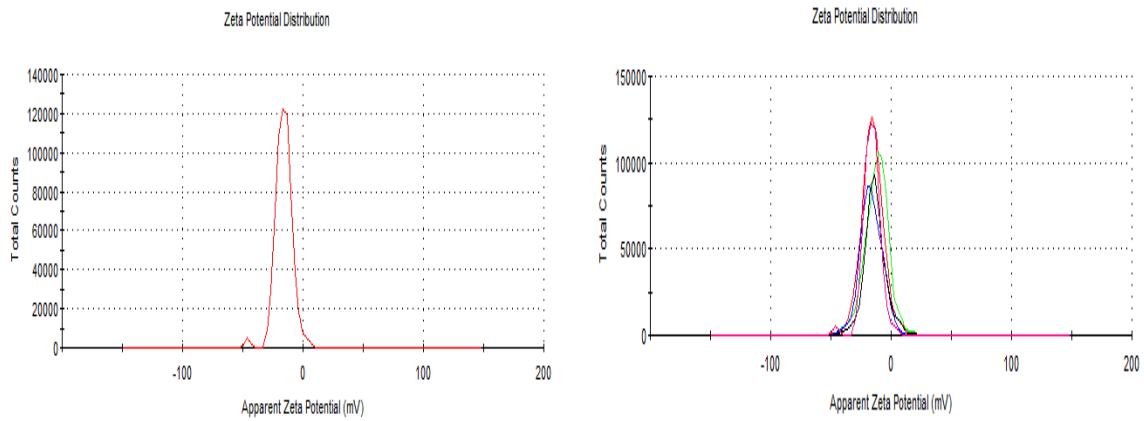

2(e) 2(f)

Fig. 2: Surface charge profiles (a to e) L-DOX A to L-DOX E and (f) Overlay of all batches.

Table 2: Size distributions and zeta potentials of doxorubicin liposomes under varying concentrations of cholesterol and β-sitosterol.

Formulation Code	Hydrodynamic Diameter (nm)	Polydispersity Index (PDI)	Zeta Potential (mV)
L-DOX A	89 ± 6	0.125 ± 0.02	-12.1 ± 4.66
L-DOX B	95 ± 5	0.093 ± 0.01	-15.6 ± 3.23
L-DOX C	99 ± 6	0.079 ± 0.04	-16.5 ± 1.92
L-DOX D	107 ± 8	0.083 ± 0.03	-13.6 ± 2.31
L-DOX E	111 ± 6	0.177 ± 0.02	-16.1 ± 2.43

3.2 Hydrodynamic Elution Profiling via Asymmetric Flow Field-Flow Fractionation

The elution profiles generated via asymmetric flow field-flow fractionation (AF4), illustrated in Fig. 3, strongly corroborate the hydrodynamic size metrics gathered from our DLS experiments and the structural features captured during Cryo-TEM imaging. For instance, the optimized L-DOX C variant produced a highly defined, largely symmetric elution peak centered around 14.9 minutes. This sharp peak exhibited a lowest width at half-maximum height, confirming notably uniform particle distribution.

On the other hand, the elution curves for L-DOX A, L-DOX B, and L-DOX D turned out much broader, showing distinct shoulders and extended trailing edges. These irregular features indicate higher physical heterogeneity or the emergence of minor secondary vesicle subpopulations within those batches[31], [32] .

From a mechanistic standpoint, embedding different sterols into a phospholipid bilayer directly dictates its mechanical stiffness, membrane ordering, and molecular packing; however, these structural outcomes depend heavily on the exact molecular design of the sterol and the base lipid matrix[33] . Consequently, the crisp, well-resolved AF4 peak recorded for L-DOX C implies that this specific ratio of ingredients achieves an optimal thermodynamic balance under

our processing environments. This hypothesis is thoroughly validated by the close harmony between our AF4 fractograms, DLS distributions, and Cryo-TEM micrographs. Taken together, these three orthogonal characterization techniques confirm that L-DOX C possesses the highest structural uniformity among all prepared groups. Securing such well-regulated physical properties represents a critical quality attribute, since vesicle size distributions and compositional uniformity heavily dictate downstream cellular uptake, systemic biodistribution, and in vivo clearance rate[34] .

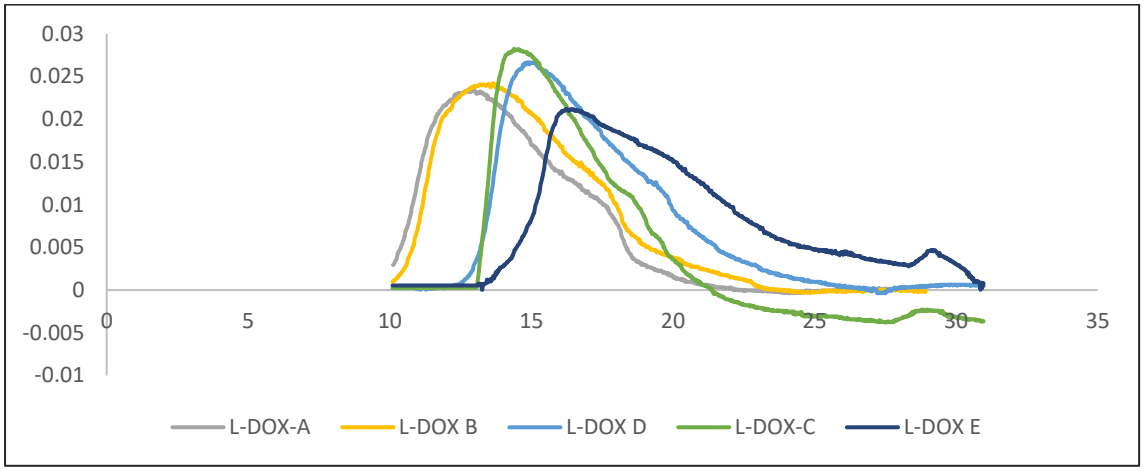

Fig. 3: Asymmetric flow field-flow fractionation (AF4) elution profiles of the engineered liposomal doxorubicin variations.

3.3 Morphological Evaluations via Cryo-TEM Imaging

We utilized cryogenic transmission electron microscopy (Cryo-TEM) to inspect the microstructural features of the five doxorubicin-loaded liposomal formulations (L-DOX A through L-DOX E). As illustrated in Fig. 4(a–e), each prepared batch predominantly comprised spherical or oval vesicular architectures defined by sharp, distinct borders. The overall architectural profile remained highly consistent across the five groups, revealing no major irregularities in vesicular geometry or membrane breakdown under our imaging conditions. These direct visual records indicate that substituting cholesterol with β-sitosterol does not trigger any drastic, easily identifiable alterations in the gross morphology of the lipid matrices.

While both cholesterol and β-sitosterol are well known to regulate phospholipid packing parameters, membrane molecular ordering, and general bilayer assembly, the subtle variances in their chemical architectures can uniquely impact their molecular cross-linking with adjacent phospholipids and subsequent membrane properties[30], [33]. Such microscale adaptations in bilayer configuration, however, often escape standard qualitative electron microscopy observation. For this reason, while the five candidate formulations display virtually identical vesicular contours on a macro-morphological level, deploying orthogonal physical characterization tools is necessary to accurately gauge finer variations in size distributions, interfacial fluidity, and long-term colloidal stability.

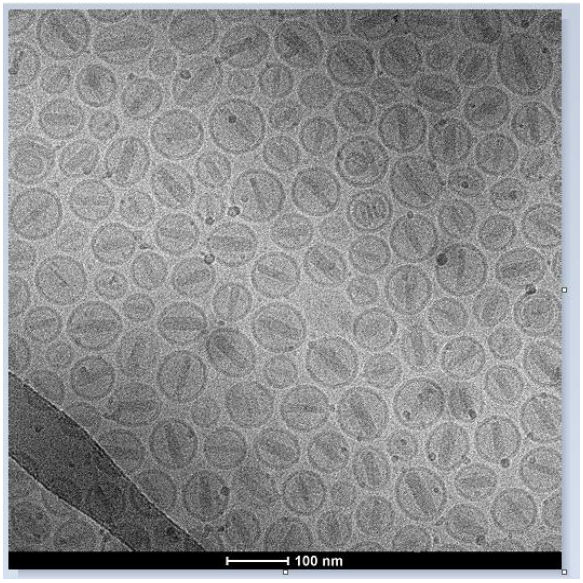

4(a)

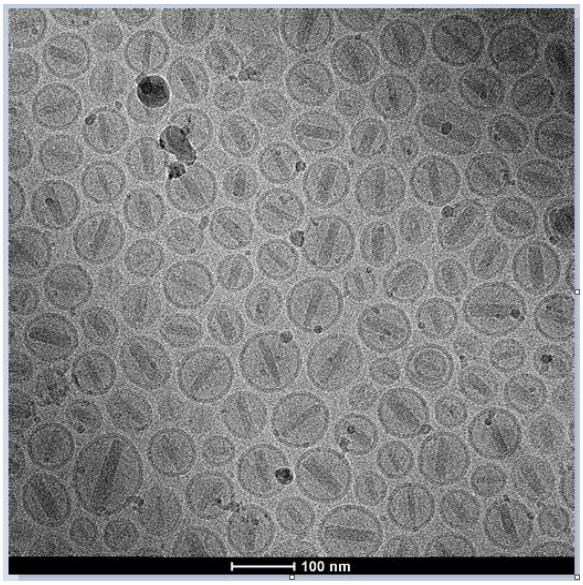

4(b)

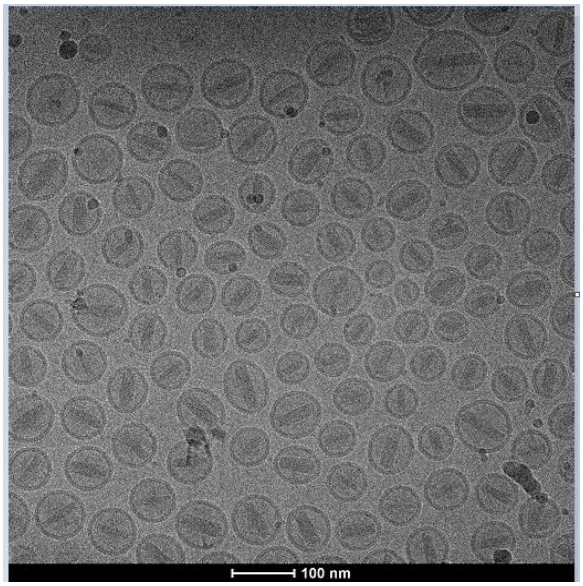

4(c)

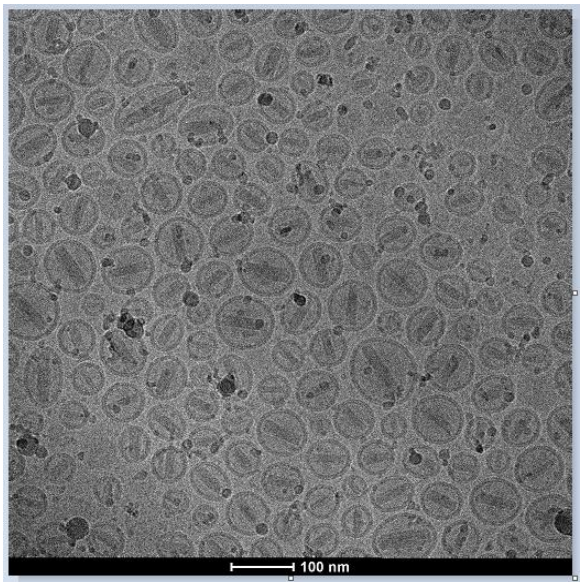

4(d)

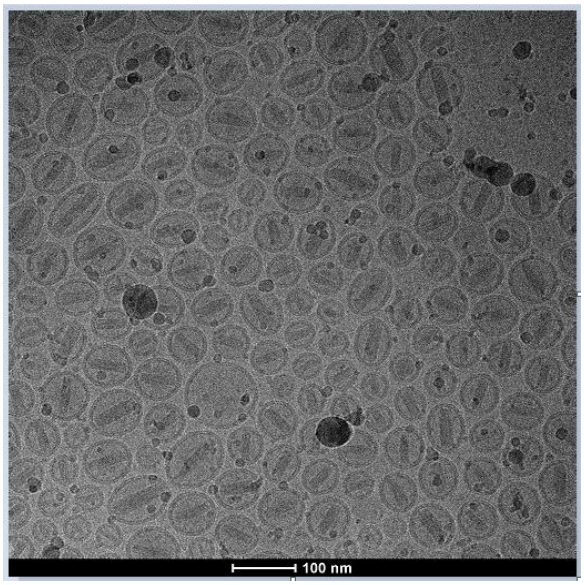

4(e)

Fig. 4: Cryo-TEM images illustrating the structural morphology of the five doxorubicin-loaded liposomal: (4a to 4e) L-DOX-A to L-DOX-E.

3.4 Evaluation of doxorubicin content and entrapment efficiency

The quantitative doxorubicin concentrations and corresponding entrapment efficiencies across our developed lipid vesicle series are summarized in Table 3. The absolute drug content was found to be tightly constrained within the narrow bounds of 99.10% to 101.03%. This tight distribution highlights excellent uniformity during loading and confirms that minimal compound loss occurred during vesicle processing. Because these recovery values mirror the theoretical input targets closely across all five lots, our analysis suggests that substituting cholesterol with β-sitosterol did not compromise the bulk drug recovery of the liposomal formulations.

Every candidate batch achieved high drug encapsulation, with trapping metrics spanning from 94.95% to 97.90%. Specifically, formulations L-DOX A, B, and C displayed remarkably comparable and optimal encapsulation efficiencies of 97.78%, 97.72%, and 97.90%, respectively. Conversely, we recorded a noticeable downward shift in trapping capacity for L-DOX D (96.49%) and L-DOX E (94.95%). This dropping encapsulation trend was closely mirrored by a complementary increase in unencapsulated doxorubicin fractions. While the free drug presence hovered around 2% for batches L-DOX A through C, it expanded to roughly 3.5% and 5.1% in the L-DOX D and E formulations, respectively.

We attribute the high core-loading yields achieved across the whole series largely to our use of the ammonium sulfate gradient-mediated remote-loading protocol. This mechanism leverages an active transmembrane ion gradient to drive the continuous influx and crystallization of doxorubicin inside the inner core, forcing excellent loading efficiency[8], [35] . The consistently high trapping values shown by L-DOX A through C indicate that these exact membrane configurations are highly compatible with this gradient-driven loading mechanism under our chosen processing states.

The lower entrapment efficiencies noted in the L-DOX D and E lots likely stem from localized reorganizations in lipid packing caused by high β-sitosterol fractions. Landmark studies have verified that altering the specific structural nature and volume fraction of embedded sterols can profoundly alter adjacent phospholipid packing density, structural fluidization, and general

interfacial layer properties[4], [5] . Thus, elevating the β-sitosterol presence likely modified the inner bilayer architecture in a way that slightly disrupted drug influx or core retention. Even so, these raw loading metrics do not conclusively prove a direct cause-and-effect relationship between sterol type and membrane permeability, meaning further analytical tracking is necessary to isolate the molecular mechanism.

Importantly, the lower entrapment values of L-DOX D and L-DOX E did not cause a matching reduction in the overall doxorubicin assay. This phenomenon reveals that the true structural divergence between these lots lies in how the active drug partitions between the trapped core and the continuous aqueous media, rather than a deficiency in total batch payload. Taken together, our data demonstrates that tuning the lipid membrane makeup can guide doxorubicin compartmentalization, underscoring that selecting a well-balanced β-sitosterol fraction is vital to achieve highly efficient core loading while optimizing overall nanocarrier profiles.

Table 3: Doxorubicin content, entrapped and free drug for all five formulations.

Formulation Code	Total Drug Content (%)	Encapsulated Fraction (%)	Unencapsulated Fraction (%)
L-DOX A	100.21	97.78	2.22
L-DOX B	100.04	97.72	2.28
L-DOX C	99.10	97.90	2.08
L-DOX D	99.85	96.49	3.51
L-DOX E	101.03	94.95	5.05

3.5 Lipid content

The lipid assay results presented in Table 4 demonstrate a consistent lipid composition across the five L-DOX formulations. HSPC was recovered at approximately 98% of its nominal content, whereas mPEG-DSPE, cholesterol, and β-sitosterol showed recoveries of approximately 99–100%. The relatively narrow variation in assay results suggests that the formulation process provided consistent levels of the lipid components across the batches examined. Determining the levels of phospholipids and other lipid constituents is necessary to establish the compositional profile of liposomal formulations and evaluate their consistency and stability[19], [20] . In particular, simultaneous measurement of the major lipid components can help verify formulation composition and identify potential deviations from the intended lipid ratios. The observed results therefore support the consistency of the measured lipid content across the five L-DOX formulations.

Table 4: Quantitative Analysis of Lipid Components in Liposomal Formulations with Varying Cholesterol and β-Sitosterol Contents

Formulation Code	% HSPC	% m-PEG DSPE	% Cholesterol	% β-Sitosterol
L-DOX A	98.21	98.78	99.82	100.54
L-DOX B	97.63	99.72	99.56	100.12
L-DOX C	98.12	99.52	100.21	101.11

L-DOX D	98.54	98.49	99.88	99.58
L-DOX E	97.91	98.95	101.12	99.88

3.6 Influence of Sterol Substitution on Bilayer Phase Transition Behavior

Nano differential scanning calorimetry (Nano DSC) was performed to evaluate the thermal transition characteristics of the developed doxorubicin-loaded liposomal formulations. The transition temperature (Tm), enthalpy change (ΔH), and two-state scaled area (Aw) were determined to assess differences in the thermal behavior of the formulations containing different proportions of cholesterol and β-sitosterol.

The transition temperatures of L-DOX-A, L-DOX-B, L-DOX-C, L-DOX-D, and L-DOX-E were 52.63, 53.20, 52.70, 52.99, and 52.84 °C, respectively. The relatively narrow temperature range (52.63–53.20 °C) indicates that the formulations exhibited similar characteristic transition temperatures. L-DOX-B showed the highest transition temperature (53.20 °C), whereas L-DOX-A showed the lowest (52.63 °C) (Table 5, Fig. 5(a) to 5(f)). The limited variation in Tm suggests that changes in sterol composition did not substantially alter the temperature associated with the observed thermal transition.

The enthalpy change varied considerably among the formulations. L-DOX-C exhibited the highest ΔH (479.0 kJ/mol), followed by L-DOX-D (451.8 kJ/mol), L-DOX-B (338.3 kJ/mol), L-DOX-A (330.9 kJ/mol), and L-DOX-E (314.8 kJ/mol). The higher enthalpy values observed for L-DOX-C and L-DOX-D indicate that a greater amount of heat was associated with their fitted thermal transitions under the experimental conditions. These differences may reflect changes in the thermal transition characteristics arising from variations in lipid–sterol interactions and bilayer organization. However, enthalpy differences alone cannot establish the relative membrane stability of the formulations.

The two-state scaled area (Aw) also showed considerable variation, ranging from 0.165 to 0.375. L-DOX-C exhibited the lowest Aw value (0.165), followed by L-DOX-D (0.180), L-DOX-A (0.331), L-DOX-B (0.335), and L-DOX-E (0.375). The differences in Aw indicate variation in the fitted two-state transition parameter among the formulations. The lower values observed for L-DOX-C and L-DOX-D, alongside their higher enthalpy values, demonstrate that these formulations exhibited distinct thermal transition characteristics compared with the other formulations.

Overall, Nano DSC analysis revealed differences in the thermal transition characteristics of the five liposomal formulations despite their relatively similar transition temperatures. L-DOX-B exhibited the highest Tm, whereas L-DOX-C exhibited the highest enthalpy change and the lowest Aw. In contrast, L-DOX-E showed the lowest enthalpy change and the highest Aw. These findings indicate that the differences among the formulations were more pronounced in enthalpy and the fitted two-state scaled area than in transition temperature. The results provide insight into the influence of formulation composition on the thermal behavior of the developed liposomal systems.

Table 5: Thermodynamic transition parameters derived from nano-differential scanning calorimetry (Nano DSC) for doxorubicin-loaded lipid nanocarriers.

Formulation Code	Phase Transition Temperature (T_m °C)	Enthalpy Change (ΔH ,kJ/mol)	Two State Scaled Area (A_w)
L-DOX A	52.63°C	330.9	0.331
L-DOX B	53.20°C	338.3	0.335
L-DOX C	52.70°C	479.0	0.165
L-DOX D	52.99°C	451.8	0.180
L-DOX E	52.84°C	314.8	0.375

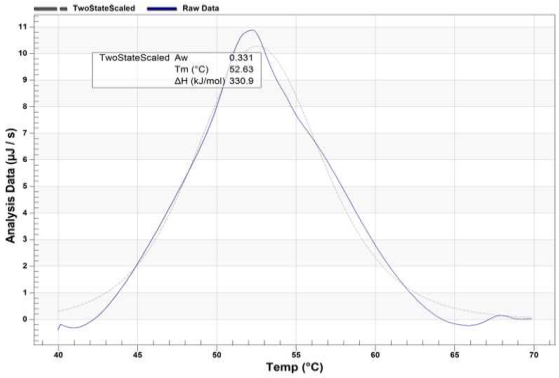

5(a)

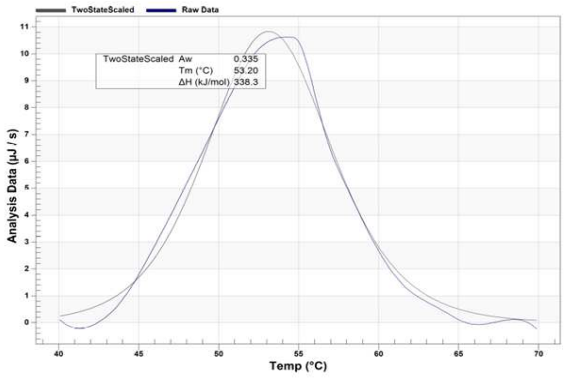

5(b)

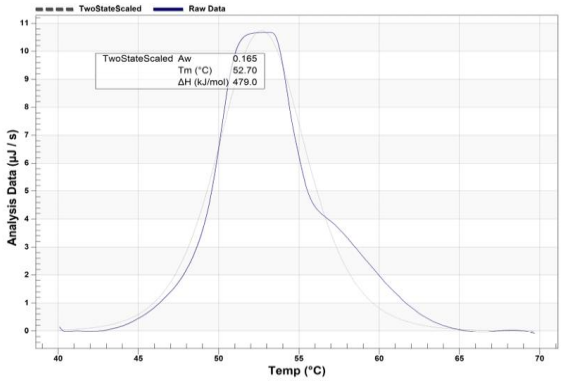

5(c)

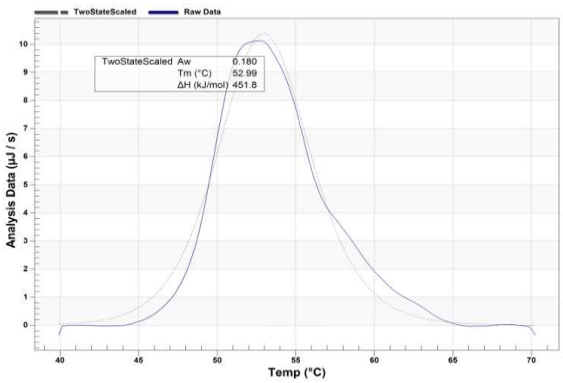

5(d)

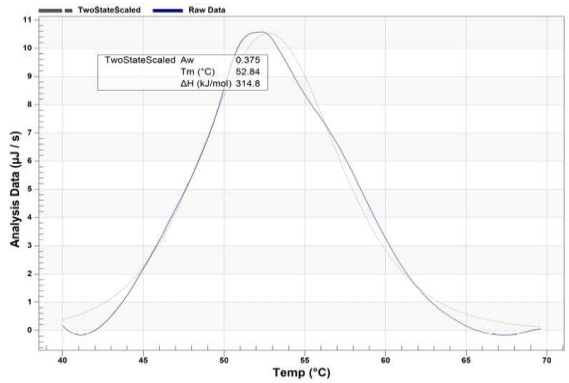

5(e)

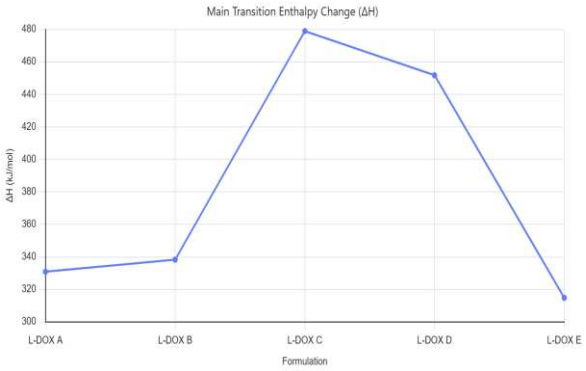

5(f)

Fig. 5: DSC thermodynamic profiles of doxorubicin-loaded lipid vesicles: (a–e) representative thermograms for formulation batches L-DOX A to L-DOX E, alongside (f) a graphical comparison of their respective enthalpy changes.

3.7 Determination of the Lyso-PC Contents

The effect of storage temperature on phospholipid degradation was evaluated by monitoring lysophosphatidylcholine (Lyso-PC) content in the five liposomal formulations over six months at 25°C. The initial Lyso-PC, detailed in Table 6, content ranged from 2.14% to 3.52% across the formulations, indicating differences in their initial phospholipid degradation profiles.

L-DOX A and L-DOX B exhibited gradual increases in Lyso-PC content during storage. In L-DOX A, the content increased from 3.52% initially to 3.65%, 4.22%, and 5.66% after 1, 3, and 6 months, respectively, as shown in Table 6. Similarly, L-DOX B showed an increase from 3.26% to 3.58%, 4.31%, and 4.99% over the same period (Table 6). These results indicate progressive Lyso-PC accumulation, although the magnitude of the increase was comparatively limited in both formulations.

L-DOX C exhibited the smallest change in Lyso-PC content, increasing from 2.45% initially to 2.81% after six months. The increase was gradual, with values of 2.55% and 2.67% at months 1 and 3, respectively. The limited increase in Lyso-PC content suggests comparatively lower accumulation of phospholipid degradation products in this formulation under the investigated storage conditions.

In contrast, the complete stability profile in Table 6 highlights that L-DOX D and L-DOX E exhibited substantial increases in Lyso-PC content during storage. L-DOX D increased from 2.14% initially to 4.85% after one month, 8.87% after three months, and 13.55% after six months. Similarly, L-DOX E increased from 2.20% to 3.98%, 9.21%, and 14.11% at the respective time points. The pronounced increases after the first month indicate that these formulations accumulated considerably more Lyso-PC during prolonged storage at 25°C than the other three formulations.

Lyso-PC formation is associated with the hydrolysis of phosphatidylcholine, the principal phospholipid component of HSPC. The differences observed among the formulations may reflect variations in lipid–sterol interactions, bilayer organization, and the susceptibility of phospholipids to hydrolysis37,38. The results suggest that the formulation composition influences Lyso-PC accumulation.

Overall, L-DOX C demonstrated the lowest Lyso-PC content throughout the six-month study, whereas L-DOX D and L-DOX E showed marked increases during storage at 25°C. L-DOX A and L-DOX B exhibited intermediate changes. These findings demonstrate formulation-dependent differences in Lyso-PC accumulation and identify L-DOX C as the formulation with the most favorable Lyso-PC profile under the investigated conditions.

Table 6: Quantification of Lyso-PC in doxorubicin-loaded liposomal formulations up to 6 months at 25°C.

Stability condition	L-DOX A (%)	L-DOX B (%)	L-DOX C (%)	L-DOX D (%)	L-DOX E (%)
Initial	3.52	3.26	2.45	2.14	2.20

1M_25°C	3.65	3.58	2.55	4.85	3.98
3M_25°C	4.22	4.31	2.67	8.87	9.21
6M_25°C	5.66	4.99	2.81	13.55	14.11

3.8 Diffusion Kinetics and Transmembrane Release Behavior of Doxorubicin

The in vitro dissolution profiles illustrated in Fig. 6 reveal a clear, composition-dependent leakage behavior for the doxorubicin-loaded vesicle series. Formulations L-DOX A and L-DOX B displayed highly similar leakage traits, leaking roughly 50% to 55% of their total drug payload within the initial 4-hour window. In sharp contrast, the optimized L-DOX C batch demonstrated a noticeably more sustained profile. While its early leakage was suppressed, its cumulative drug delivery ultimately climbed to 92% by the 24-hour mark, indicating that this specific matrix induces a targeted delay during the initial burst window rather than reducing the final, long-term elution capacity.

Conversely, batches L-DOX D and L-DOX E underwent rapid drug leakage, discharging nearly 78% to 80% of their core payload within just 4 hours and nearing complete elution (95% to 98%) by hours 6 to 8. These trends reveal that increasing the β-sitosterol fraction does not create a simple linear decrease in drug delivery rates. Instead, the equal-mass integration of cholesterol and β-sitosterol achieved in the L-DOX C framework was uniquely tied to the most controlled early-phase release among all tested variations.

These structural variations likely stem from modifications in the phospholipid bilayer arrangement and subsequent core retention properties dictated by the specific sterol blending ratios. Although both cholesterol and β-sitosterol alter the physical boundaries of phospholipid-based thin films, their collective structural impact depends heavily on the surrounding lipid environment and cannot be anticipated purely through individual component volumes[4], [33] . Consequently, the delayed transport kinetics recorded for L-DOX C points to an optimized lipid-packing configuration or enhanced affinity for the core-bound doxorubicin molecular structure.

By the conclusion of the 24-hour experimental timeline, all candidate lots converged to show an overlapping 94% to 97% cumulative drug release. This convergence proves that the primary kinetic variations between these matrices are restricted to the early and intermediate diffusion phases. Taken together, our data shows that adjusting the cholesterol to β-sitosterol balance controls the underlying elution mechanics of doxorubicin under simulated physiological states. The slower early-stage diffusion seen in L-DOX C is likely governed by a highly ordered, mechanically rigid lipid network optimized by its specific sterol ratio. Tightening this lipid packing lowers the overall cross-sectional permeability of the membrane, limiting free drug transport across the bilayer boundary. From a clinical perspective, this sustained delivery pattern makes L-DOX C highly advantageous, as extending the drug release window helps maintain steady therapeutic levels over a prolonged timeframe while dampening maximum peak plasma concentrations to avoid off-target side effects[36], [37] .

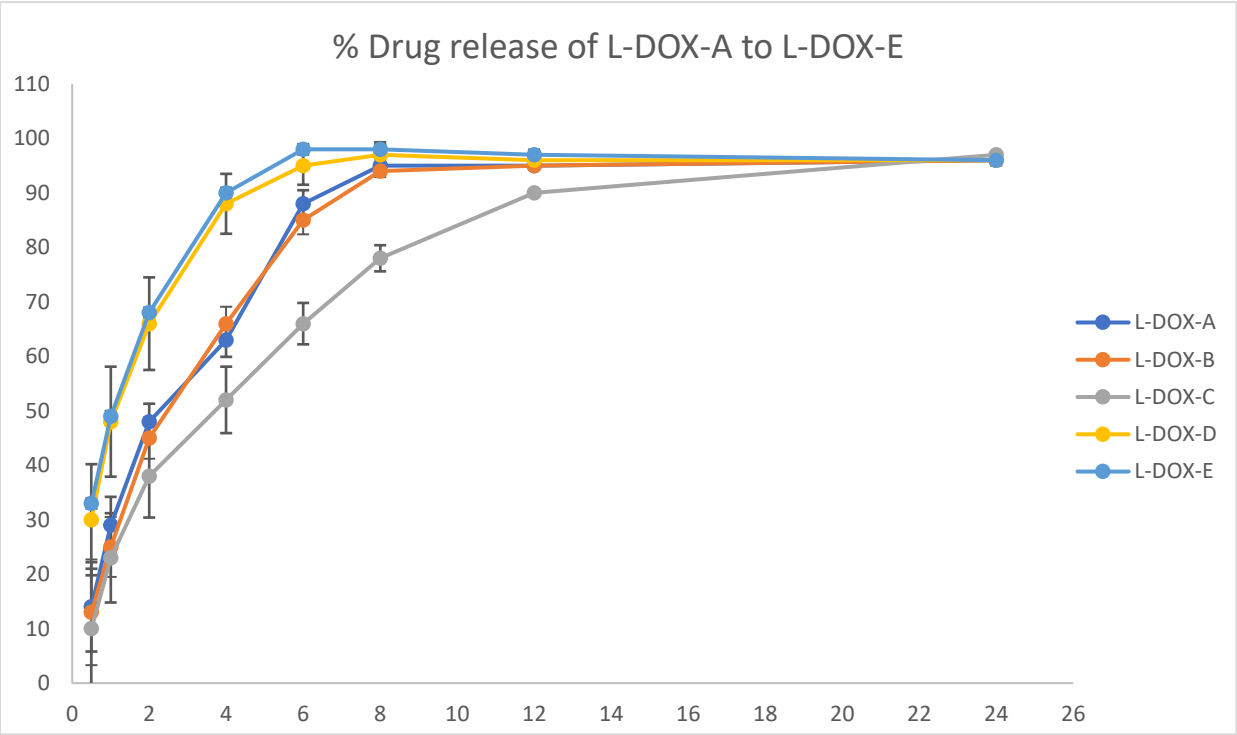

Fig. 6: In vitro drug release kinetics of the doxorubicin-loaded liposomal variations: individual dissolution profiles track formulations L-DOX A through L-DOX E over a 24-hour testing window. Relative percent coefficient of variation (% CV) margins are marked across each collection interval (n = 3).

3.9 In Vitro Scratch Assay and Cellular Motility Evaluation

Our in vitro scratch assay (Fig. 7) revealed that the optimized L-DOX C formulation exerts a powerful anti-migratory effect on MCF-7 breast cancer cells. Within a 24-hour incubation window, the untreated control cells migrated aggressively, nearly closing the denuded scratch zone entirely. Conversely, the cell populations exposed to L-DOX C displayed minimal boundary migration and wound closure, demonstrating a profound suppression of active cellular locomotion.

From a biochemical standpoint, we primarily attribute this severe restriction in cell motility to doxorubicin's established mechanism of action: its ability to intercalate into genomic DNA and block topoisomerase II activity. This interaction disrupts the downstream transcriptional cascades and structural signaling networks that driving tumor cell movement. Furthermore, the co-encapsulated β-sitosterol likely provides a synergistic benefit here, given its documented role in limiting metastatic cellular behaviors. Taken together, these scratch-healing outcomes prove that the L-DOX C architecture acts as an effective blocker of cancer cell migration a key prerequisite for systemic tumor spread thereby emphasizing its potential as a targeted anti-metastatic intervention.

Untreated Wells

T=0Hrs T=24Hrs

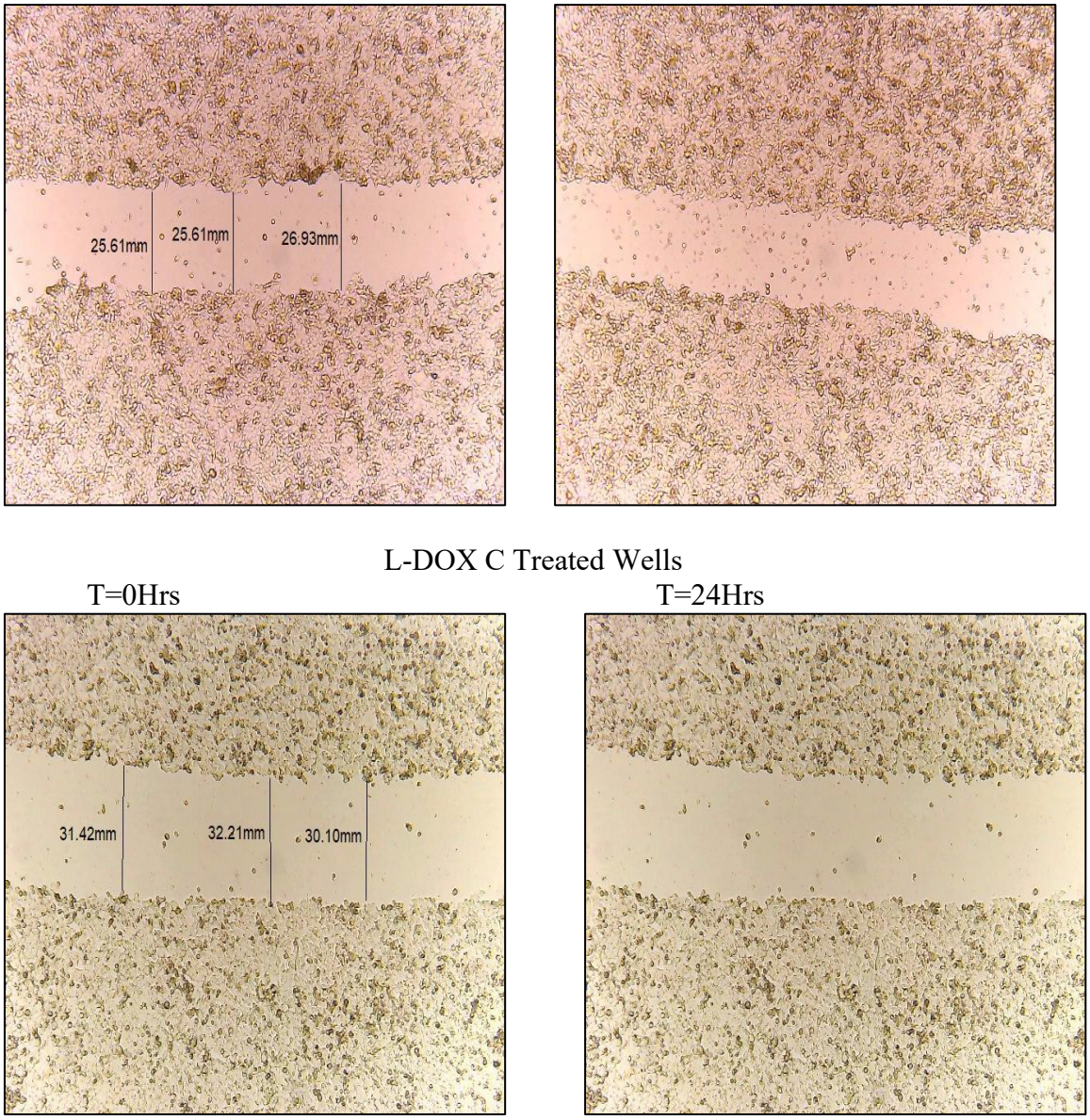

Fig. 7: Scratch-healing images of MCF-7 cultures: representative microscopic fields for without treatment and L-DOX C-treated monolayers at 0 and 24 hours in the migration assay.

3.10 Dose-Dependent Antiproliferative Action and In Vitro Cytotoxicity

Our in vitro cell viability investigations using MCF-7 breast cancer cultures demonstrated that the optimized L-DOX C formulation possesses a significantly higher antiproliferative potency than the commercial liposomal doxorubicin control. Specifically, the calculated IC_{50} value for L-DOX C was found to be 1174 nM, a substantial drop compared to the 2420 nM recorded for the marketed product benchmark [Fig.s 8(a) and 8(b)]. At a high doxorubicin concentration of 10,000 nM, exposure to L-DOX C induced a massive 92.29% suppression of tumor cell viability, whereas the commercial formulation achieved a lower inhibition rate of 84.88% across the same timeline [Fig. 9 and Fig. 10]. Furthermore, direct microscopic examination of the MTT assay wells [Fig. 9 and Fig. 10] provided visual proof of these trends, revealing severe cellular shape distortion and a marked collapse in living cell density within the L-DOX C treatment groups compared to both the unexposed controls and the commercial liposomal variations.

These combined findings suggest that the specific nanoscale architecture of L-DOX C which features reinforced lipid bilayer stability alongside a highly regulated, sustained drug release profile improves intracellular drug accumulation. This optimized delivery mechanic directly enhances therapeutic efficiency, particularly at lower dose thresholds. The pronounced reduction in the IC_{50} limit paired with the escalated growth inhibition documented at 10,000 nM strongly implies that our engineered L-DOX C vesicles can secure superior overall tumor eradication relative to conventional, commercially available formulations.

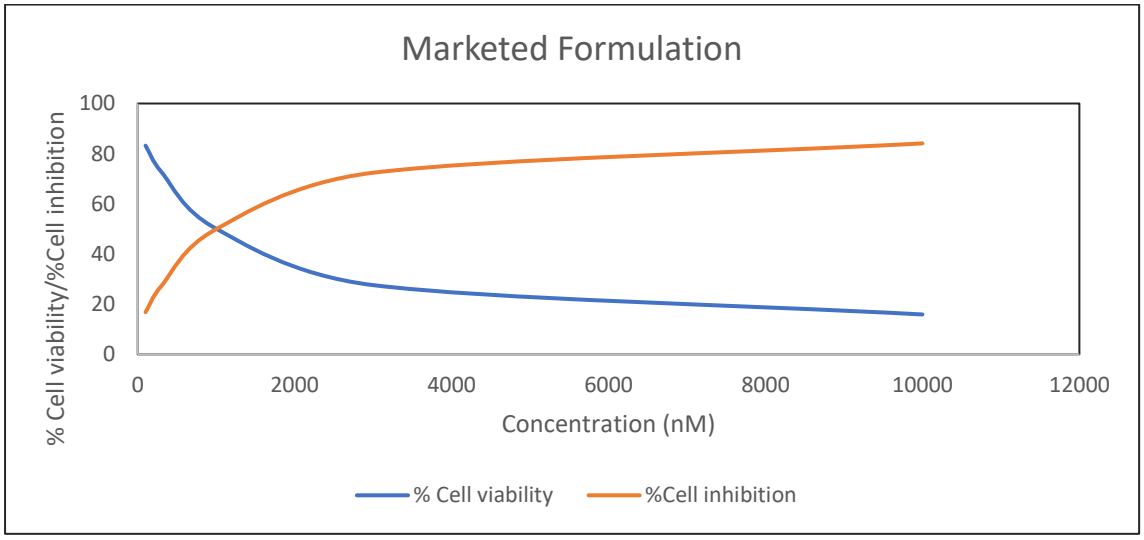

8(a)

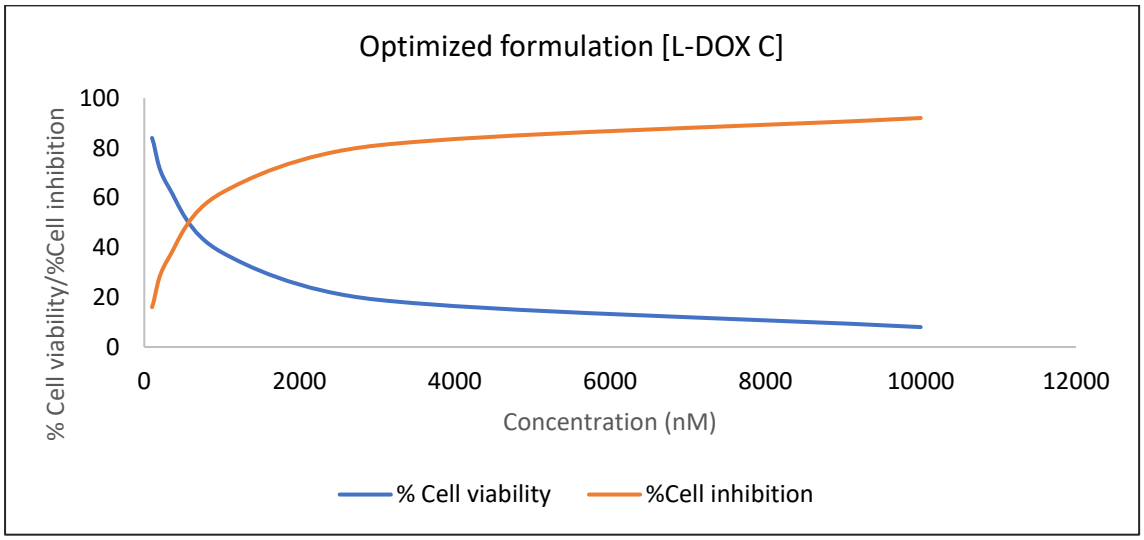

8(b)

Fig. 8: Dose-dependent profiles mapping the relationship between active drug concentrations and cell viability/growth inhibition parameters. Curves outline the performance of (a) the Marketed Formulation and (b) our optimized variant (L-DOX C). Optical density values were tracked at an absorbance wavelength of 570 nm using the MTT colorimetric assay in MCF-7 human breast cancer lines.

Before treatment After treatment 100 nM

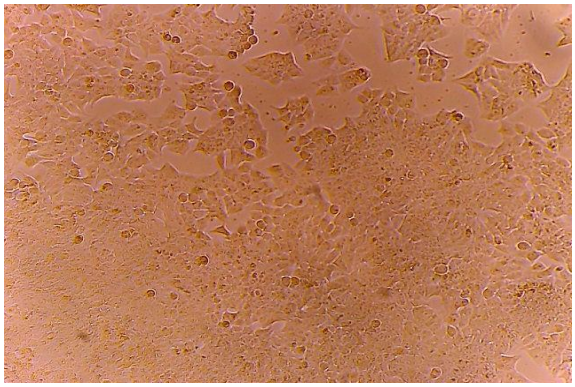

After treatment 300 nM

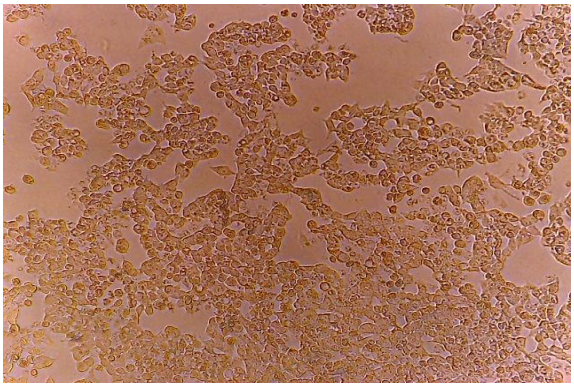

After treatment 1000 nM

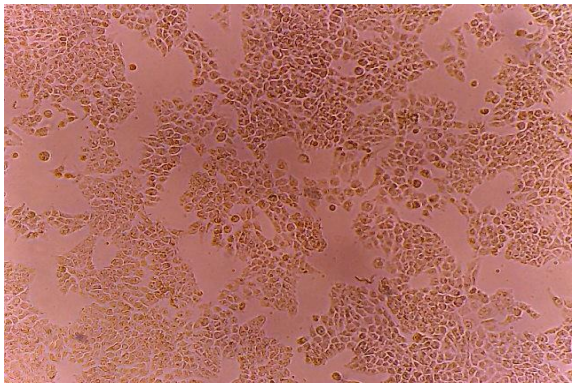

After treatment 3000 nM

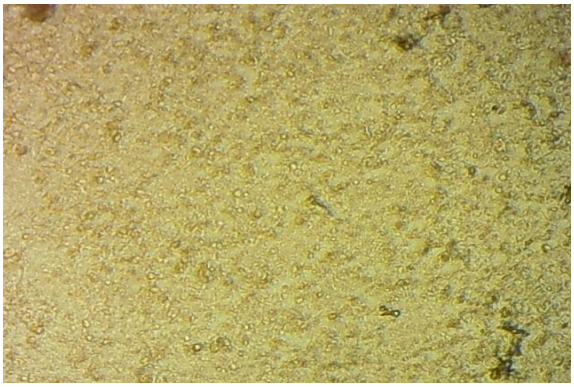

After treatment 10000 nM



Before Treatment

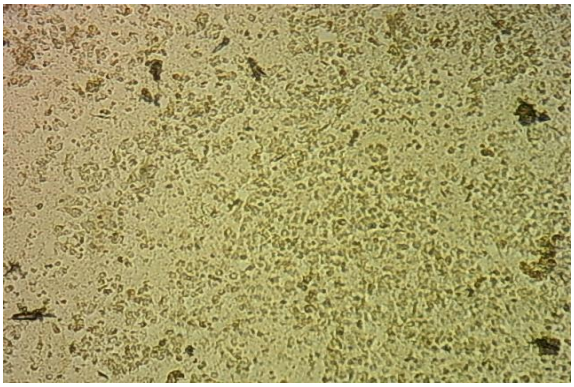

After treatment 100 nM

Fig. 9: Microscopic visualization of cellular changes in MCF-7 cultures induced by the commercial liposomal doxorubicin control. Representative fields illustrate the cytotoxic response across various concentration thresholds.

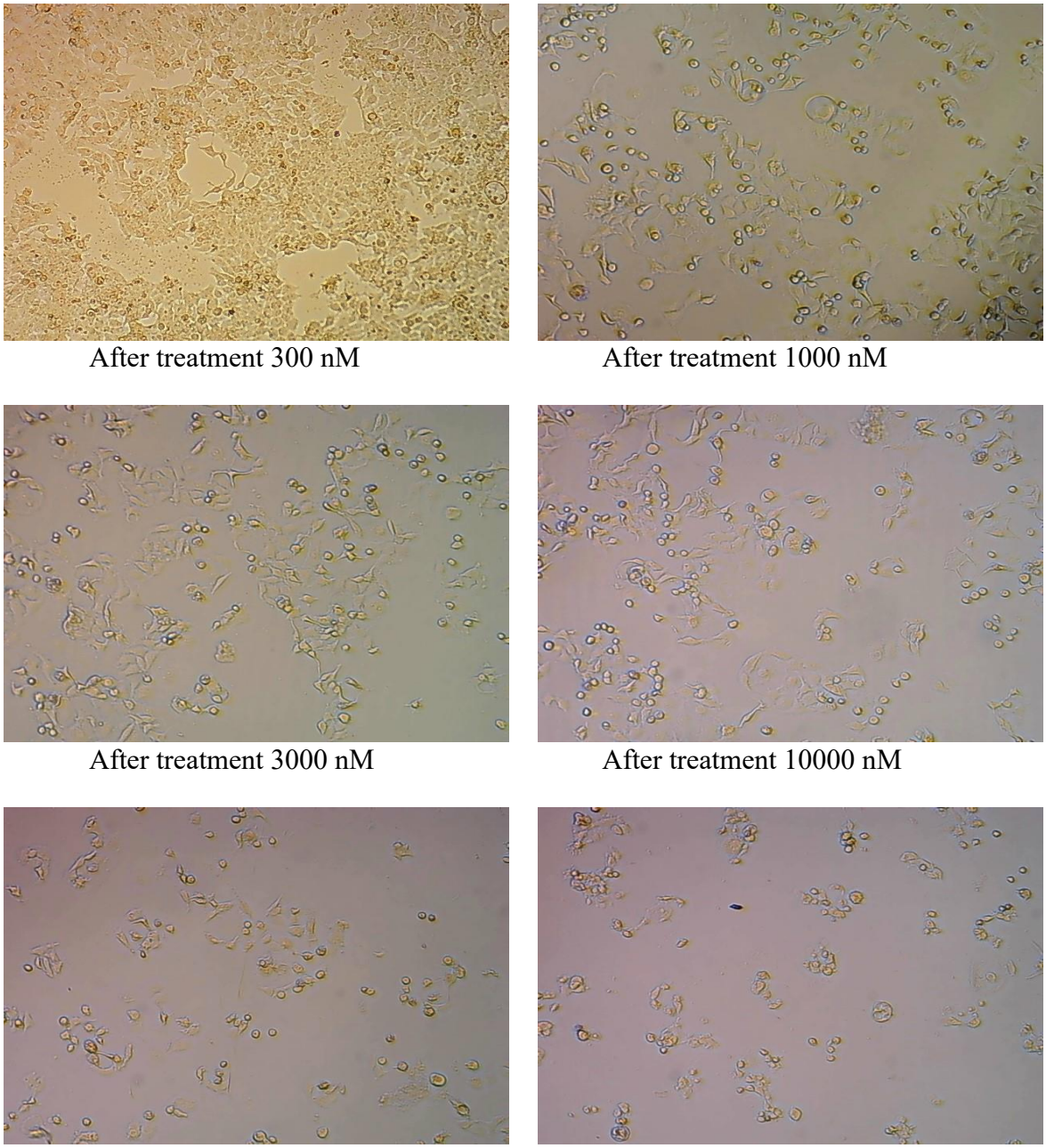

Fig. 10: Microscopic visualization of cellular changes in MCF-7 cultures induced by the engineered sterol-modified vesicles. Representative fields illustrate the cytotoxic response across various concentration thresholds.

3.11 Serum Compatibility and Structural Robustness in Human Plasma Matrices

Our plasma stability assessments indicated that after a full 24-hour incubation timeline at 37 °C, the cumulative leakage of doxorubicin was restricted to approximately 17%, while the hydrodynamic size profile of the nanocarriers remained remarkably uniform (Tables 7 and 8).

These quantitative trends confirm that the engineered liposomal matrix successfully preserves its structural architecture and retains the vast majority of its active molecular payload when exposed to complex biological fluids. Consequently, this high structural integrity supports the

formulation's capacity to maintain prolonged circulation lifetimes and ensure predictable, controlled release rates under real physiological environments.

Table 7: Evaluation of hydrodynamic diameter fluctuations during incubation in human plasma (37 °C).

Exposure Timeline	Mean Hydrodynamic Diameter (Z avg, nm)
0 h	100 ± 6
2 h	98 ± 7
4 h	103 ± 4
6 h	101 ± 5
8 h	102 ± 8
12 h	100 ± 7
24 h	101 ± 6

Note: All physical dimensions are expressed as the mean ± standard deviation derived from independent triplicate evaluations (n = 3).

Table 8: % Encapsulated vs. unencapsulated doxorubicin fractions in plasma over time.

Exposure Timeline	Unencapsulated Fraction (% Free Drug)	Encapsulated Fraction (% Entrapped Drug)
0 h	3.13 ± 1.01	96.87 % ± 2.02
2 h	7.41 ± 0.38	92.59 % ± 1.07
4 h	7.51 ± 0.52	92.49 % ± 1.89
6 h	9.29 ± 1.15	90.71 % ± 1.51
8 h	11.25 ± 0.81	88.75 % ± 2.03
12 h	13.61 ± 1.50	86.39 % ± 0.78
24 h	17.42 ± 1.11	82.58 % ± 1.02

Note: Values denote the mean percentage mass distribution ± standard deviation (n = 3) tracking drug partitioning behavior at a simulated physiological temperature of 37 °C.

4.0 CONCLUDING REMARKS AND FUTURE OUTLOOK

In summary, this investigation highlights that the strategic substitution of cholesterol with β-sitosterol serves as an effective mechanism to optimize liposomal doxorubicin delivery vehicles. Integrating β-sitosterol encourages a highly ordered bilayer layout and tighter intermolecular lipid packing. This structural modification effectively reduces unwanted water permeation into the membrane core and suppresses specific hydrolytic breakdown pathways,

such as those leading to Lyso-PC impurity formation.

This reinforced membrane structure completely stops the rapid, uncontrolled drug dumping often observed in unstable liposomal designs. Instead, it promotes a smooth, diffusion-controlled release profile that spans past 24 hours, regulated by the tightly packed lipid boundaries. Furthermore, this superior structural configuration ensures high core-loading efficiency paired with excellent batch-to-batch reproducibility with all fundamental membrane components tracking between 98% and 101% of theoretical targets offering great promise for scaled industrial production.

From a biological standpoint, the optimized L-DOX C formulation demonstrated superior antiproliferative potency against MCF-7 human breast cancer cells, securing a significantly enhanced cytotoxicity profile over the standard commercial alternative IC_{50} of 1174 nM versus 2420 nM). Additionally, L-DOX C actively blocked cancer cell migration pathways and demonstrated excellent durability in human plasma, suffering no major size shifts or payload loss after 24 hours of exposure. Ultimately, this straightforward sterol-replacement approach yields an advanced liposomal nanocarrier system that combines enhanced shelf stability, controlled drug delivery kinetics, and powerful anti-cancer efficacy for reliable oncological therapy.

5.0 LIST OF ABBREVIATIONS AND ACRONYMS

- **AF4 –** Asymmetric Flow Field-Flow Fractionation
- **ANOVA –** Analysis of Variance
- **Aw –** Two-State Scaled Melting Area Parameter
- **BS –** β-Sitosterol Phytosterol Component
- **Cryo-TEM –** Cryogenic Transmission Electron Microscopy
- **CV –** Coefficient of Variation Percentage
- **DLS –** Dynamic Light Scattering Analytical Technique
- **DMEM –** Dulbecco's Modified Eagle Medium (Cell Culture Matrix)
- **DMSO –** Dimethyl Sulfoxide Solubilization Agent
- **DOX –** Doxorubicin Hydrochloride
- **DSPG-Na –** 1,2-distearoyl-sn-glycero-3-phosphoglycerol sodium salt configuration
- **FBS –** Fetal Bovine Serum Supplement
- **GRAS –** Generally Recognized as Safe Regulatory Classification
- **HPLC –** High-Performance Liquid Chromatography
- **HPLC-RI –** High-Performance Liquid Chromatography with Refractive Index Detection
- **HSPC –** Hydrogenated Soy Phosphatidylcholine
- **IC_{50} –** Half-Maximal Inhibitory Concentration Value
- **Lyso-PC –** Lysophosphatidylcholine Degradation Matrix
- **MTT –** 3-(4,5-dimethylthiazol-2-yl)-2,5-diphenyl tetrazolium bromide assay reagent
- **Nano-DSC –** Nano-Differential Scanning Calorimetry
- **PBS –** Phosphate-Buffered Saline Buffer Environment
- **PDI –** Polydispersity Index Evaluation
- **RI –** Refractive Index Detection Parameter
- **SD –** Standard Deviation
- **Δ H –** Net Enthalpy Change Indicator
- **Tm –** Core Phase Transition Temperature
- **UV/Vis –** Ultraviolet-Visible Spectroscopy Detector

6.0 DECLARATIONS

Acknowledgements

The authors gratefully credit The Parul University, Vadodara, and Sun Pharma R & D Centre, Vadodara, for the essential facilities and resources required to carry out this research activity.

Author Contribution Statement

- **Bhavin Dave:** Research Design, Formal Analysis, Data Curation, Experimental Methodology, Graphical Visualization, Manuscript Preparation - Original Draft.
- **Avik Parekh:** Manuscript Evaluation - Review and Refinement.
- **Dr. Rajesh Dodiya:** Conceptual Design, Academic Supervision, Project Coordination.

Funding

The authors declare that no external funding, grants, or financial support from public or commercial agencies was received for the execution of this study.

Data Availability Statement

The primary datasets generated and analyzed during the current investigation are available from the corresponding author upon reasonable academic request.

Conflict of Interest / Competing Interests

The authors declare that they have no personal, commercial, financial, or non-financial conflicts of interest linked to the execution or publication of this research article.

Ethics Approval and Consent to Participate

This article does not contain any studies involving human participants or animal subjects performed by any of the authors.

7.0 REFERENCES

[1] Y. Octavia, C. G. Tocchetti, K. L. Gabrielson, S. Janssens, H. J. Crijns, and A. L. Moens, "Doxorubicin-induced cardiomyopathy: From molecular mechanisms to therapeutic strategies," *J. Mol. Cell. Cardiol.*, vol. 52, no. 6, pp. 1213–1225, Jun. 2012, doi: 10.1016/j.yjmcc.2012.03.006.

[2] C. Carvalho *et al.*, "Doxorubicin: The Good, the Bad and the Ugly Effect," *Curr. Med. Chem.*, vol. 16, no. 25, pp. 3267–3285, Sep. 2009, doi: 10.2174/092986709788803312.

[3] U. Bulbake, S. Doppalapudi, N. Kommineni, and W. Khan, "Liposomal Formulations in Clinical Use: An Updated Review," *Pharmaceutics*, vol. 9, no. 2, p. 12, Mar. 2017, doi: 10.3390/pharmaceutics9020012.

[4] A. A. Jovanović *et al.*, "Comparative Effects of Cholesterol and β-Sitosterol on the Liposome Membrane Characteristics," *European Journal of Lipid Science and Technology*, vol. 120, no. 9, Sep. 2018, doi: 10.1002/ejlt.201800039.

[5] F. Song, J. Chen, A. Zheng, and S. Tian, “Effect of sterols on liposomes: Membrane characteristics and physicochemical changes during storage,” *LWT*, vol. 164, Jul. 2022, doi: 10.1016/j.lwt.2022.113558.

[6] A. Gouda, O. S. Sakr, M. Nasr, and O. Sammour, “Ethanol injection technique for liposomes formulation: An insight into development, influencing factors, challenges and applications,” *J. Drug Deliv. Sci. Technol.*, vol. 61, p. 102174, Feb. 2021, doi: 10.1016/j.jddst.2020.102174.

[7] E. M. Bolotin *et al.*, “Ammonium Sulfate Gradients for Efficient and Stable Remote Loading of Amphipathic Weak Bases into Liposomes and Ligandoliposomes.,” *J. Liposome Res.*, vol. 4, no. 1, pp. 455–479, Jan. 1994, doi: 10.3109/08982109409037057.

[8] G. Haran, R. Cohen, L. K. Bar, and Y. Barenholz, “Transmembrane ammonium sulfate gradients in liposomes produce efficient and stable entrapment of amphipathic weak bases.,” *Biochim. Biophys. Acta*, vol. 1151, no. 2, pp. 201–15, Sep. 1993, doi: 10.1016/0005-2736(93)90105-9.

[9] M. Danaei *et al.*, “Impact of Particle Size and Polydispersity Index on the Clinical Applications of Lipidic Nanocarrier Systems,” *Pharmaceutics*, vol. 10, no. 2, p. 57, May 2018, doi: 10.3390/pharmaceutics10020057.

[10] M. Danaei *et al.*, “Probing nanoliposomes using single particle analytical techniques: effect of excipients, solvents, phase transition and zeta potential,” *Heliyon*, vol. 4, no. 12, p. e01088, Dec. 2018, doi: 10.1016/j.heliyon.2018.e01088.

[11] M. Wagner, S. Holzschuh, A. Traeger, A. Fahr, and Ulrich. S. Schubert, “Asymmetric Flow Field-Flow Fractionation in the Field of Nanomedicine,” *Anal. Chem.*, vol. 86, no. 11, pp. 5201–5210, Jun. 2014, doi: 10.1021/ac501664t.

[12] S. Hupfeld, D. Ausbacher, and M. Brandl, “Asymmetric flow field-flow fractionation of liposomes: optimization of fractionation variables,” *J. Sep. Sci.*, vol. 32, no. 9, pp. 1465–1470, May 2009, doi: 10.1002/jssc.200800626.

[13] M. Almgren, K. Edwards, and G. Karlsson, “Cryo transmission electron microscopy of liposomes and related structures,” *Colloids Surf. A Physicochem. Eng. Asp.*, vol. 174, no. 1–2, pp. 3–21, Nov. 2000, doi: 10.1016/S0927-7757(00)00516-1.

[14] D. Mehn *et al.*, “Analytical ultracentrifugation for analysis of doxorubicin loaded liposomes,” *Int. J. Pharm.*, vol. 523, no. 1, pp. 320–326, May 2017, doi: 10.1016/j.ijpharm.2017.03.046.

[15] S. Deshpande, M. Farooqui, G. Sanap, and D. D. Kayande, “Development and validation of a sensitive reversed phase HPLC method to determine total, free drug and encapsulation efficiency of cytotoxic Nano pharmaceutical,” *Int. J. Pharmtech Res.*, vol. 12, no. 01, pp. 69–79, 2019, doi: 10.20902/IJPTR.2019.120110.

[16] H. Shibata, C. Yomota, and H. Okuda, “Simultaneous Determination of Polyethylene Glycol-Conjugated Liposome Components by Using Reversed-Phase High-Performance Liquid Chromatography with UV and Evaporative Light Scattering Detection,” *AAPS PharmSciTech*, vol. 14, no. 2, pp. 811–817, Jun. 2013, doi: 10.1208/s12249-013-9967-8.

[17] M. Oswald, M. Platscher, S. Geissler, and A. Goepferich, “HPLC analysis as a tool for assessing targeted liposome composition,” *Int. J. Pharm.*, vol. 497, no. 1–2, pp. 293–300, Jan. 2016, doi: 10.1016/j.ijpharm.2015.11.014.

[18] C. Demetzos, “Differential Scanning Calorimetry (DSC): A Tool to Study the Thermal Behavior of Lipid Bilayers and Liposomal Stability,” *J. Liposome Res.*, vol. 18, no. 3, pp. 159–173, Jan. 2008, doi: 10.1080/08982100802310261.

[19] M. Grit, D. J. A. Crommelin, and J. Lang, “Determination of phosphatidylcholine, phosphatidylglycerol and their lyso forms from liposome dispersions by high-performance liquid chromatography using high-sensitivity refractive index detection,” *J. Chromatogr. A*, vol. 585, no. 2, pp. 239–246, Nov. 1991, doi: 10.1016/0021-9673(91)85083-R.

[20] D. Jeschek, G. Lhota, J. Wallner, and K. Vorauer-Uhl, “A versatile, quantitative analytical method for pharmaceutical relevant lipids in drug delivery systems,” *J. Pharm. Biomed. Anal.*, vol. 119, pp. 37–44, Feb. 2016, doi: 10.1016/j.jpba.2015.11.020.

[21] H. Shibata, K. Izutsu, C. Yomota, H. Okuda, and Y. Goda, “Investigation of factors affecting *in vitro* doxorubicin release from PEGylated liposomal doxorubicin for the development of *in vitro* release testing conditions,” *Drug Dev. Ind. Pharm.*, vol. 41, no. 8, pp. 1376–1386, Aug. 2015, doi: 10.3109/03639045.2014.954582.

[22] L. Gómez-Lázaro, C. Martín-Sabroso, J. Aparicio-Blanco, and A. I. Torres-Suárez, “Assessment of In Vitro Release Testing Methods for Colloidal Drug Carriers: The Lack of Standardized Protocols,” *Pharmaceutics*, vol. 16, no. 1, p. 103, Jan. 2024, doi: 10.3390/pharmaceutics16010103.

[23] C.-C. Liang, A. Y. Park, and J.-L. Guan, “In vitro scratch assay: a convenient and inexpensive method for analysis of cell migration in vitro,” *Nat. Protoc.*, vol. 2, no. 2, pp. 329–333, Feb. 2007, doi: 10.1038/nprot.2007.30.

[24] S. K. Shukla *et al.*, “Metformin-Encapsulated Liposome Delivery System: An Effective Treatment Approach against Breast Cancer,” *Pharmaceutics*, vol. 11, no. 11, p. 559, Oct. 2019, doi: 10.3390/pharmaceutics11110559.

[25] B. Sabeti, M. I. Noordin, S. Mohd, R. Hashim, A. Dahlan, and H. Akbari Javar, “Development and Characterization of Liposomal Doxorubicin Hydrochloride with Palm Oil,” *Biomed Res. Int.*, vol. 2014, pp. 1–6, 2014, doi: 10.1155/2014/765426.

[26] T. Mosmann, “Rapid colorimetric assay for cellular growth and survival: Application to proliferation and cytotoxicity assays,” *J. Immunol. Methods*, vol. 65, no. 1–2, pp. 55–63, Dec. 1983, doi: 10.1016/0022-1759(83)90303-4.

[27] D. Patel and N. Patel, “Fabrication and characterization of sterically stabilized liposomes of topotecan,” *Futur. J. Pharm. Sci.*, vol. 6, no. 1, p. 79, Dec. 2020, doi: 10.1186/s43094-020-00089-z.

[28] M. Fazel, M. Daeihamed, M. Osouli, A. Almasi, A. Haeri, and S. Dadashzadeh, “Preparation, In-Vitro Characterization and Pharmacokinetic Evaluation of Brij Decorated Doxorubicin Liposomes as a Potential Nanocarrier for Cancer Therapy.,” *Iran. J. Pharm. Res.*, vol. 17, no. Suppl2, pp. 33–43, 2018.

[29] A. Yavlovich, A. Singh, R. Blumenthal, and A. Puri, “A novel class of photo-triggerable liposomes containing DPPC:DC8,9PC as vehicles for delivery of doxorubcin to cells,” *Biochimica et Biophysica Acta (BBA) - Biomembranes*, vol. 1808, no. 1, pp. 117–126, Jan. 2011, doi: 10.1016/j.bbamem.2010.07.030.

[30] S. Bhattacharjee, “DLS and zeta potential - What they are and what they are not?,” Aug. 10, 2016, *Elsevier B.V.* doi: 10.1016/j.jconrel.2016.06.017.

[31] J. Parot, F. Caputo, D. Mehn, V. A. Hackley, and L. Calzolai, “Physical characterization of liposomal drug formulations using multi-detector asymmetrical-flow field flow

fractionation," *Journal of Controlled Release*, vol. 320, pp. 495–510, Apr. 2020, doi: 10.1016/j.jconrel.2020.01.049.

[32] S. M. Ansar and T. Mudalige, "Characterization of doxorubicin liposomal formulations for size-based distribution of drug and excipients using asymmetric-flow field-flow fractionation (AF4) and liquid chromatography-mass spectrometry (LC-MS)," *Int. J. Pharm.*, vol. 574, p. 118906, Jan. 2020, doi: 10.1016/j.ijpharm.2019.118906.

[33] A. Hodzic, M. Rappolt, H. Amenitsch, P. Laggner, and G. Pabst, "Differential Modulation of Membrane Structure and Fluctuations by Plant Sterols and Cholesterol," *Biophys. J.*, vol. 94, no. 10, pp. 3935–3944, May 2008, doi: 10.1529/biophysj.107.123224.

[34] B. Sheikholeslami, N. W. Lam, K. Dua, and M. Haghi, "Exploring the impact of physicochemical properties of liposomal formulations on their in vivo fate.," *Life Sci.*, vol. 300, p. 120574, Jul. 2022, doi: 10.1016/j.lfs.2022.120574.

[35] A. Fritze, F. Hens, A. Kimpfler, R. Schubert, and R. Peschka-Süss, "Remote loading of doxorubicin into liposomes driven by a transmembrane phosphate gradient," *Biochimica et Biophysica Acta (BBA) - Biomembranes*, vol. 1758, no. 10, pp. 1633–1640, Oct. 2006, doi: 10.1016/j.bbamem.2006.05.028.

[36] D. Solomon, N. Gupta, N. S. Mulla, S. Shukla, Y. A. Guerrero, and V. Gupta, "Role of In Vitro Release Methods in Liposomal Formulation Development: Challenges and Regulatory Perspective," *AAPS J.*, vol. 19, no. 6, pp. 1669–1681, Nov. 2017, doi: 10.1208/s12248-017-0142-0.

[37] M. Amin, A. L. B. Seynhaeve, M. Sharifi, M. Falahati, and T. L. M. ten Hagen, "Liposomal Drug Delivery Systems for Cancer Therapy: The Rotterdam Experience," *Pharmaceutics*, vol. 14, no. 10, p. 2165, Oct. 2022, doi: 10.3390/pharmaceutics14102165.